Physically-Retrieving Cloud and Thermodynamic Parameters from Ultraspectral IR Measurements

Daniel K. Zhou,[1] William L. Smith, Sr.,[2, 3] Xu Liu,[1] Allen M. Larar,[1] Stephen A. Mango,[4] and Hung-Lung Huang[3]

[1]NASA Langley Research Center, Hampton, Virginia
[2]Hampton University, Hampton, Virginia
[3]University of Wisconsin – Madison, Madison, Wisconsin
[4]NPOESS Integrated Program Office, Silver Spring, Maryland

Manuscript submitted to *J. Atmos. Sci.*

13 February 2006.

Corresponding author:
Daniel K. Zhou
Mail stop 401A, NASA Langley Research Center, Hampton, VA 23681
Daniel.k.zhou@nasa.gov

ABSTRACT

A physical inversion scheme has been developed, dealing with cloudy as well as cloud-free radiance observed with ultraspectral infrared sounders, to simultaneously retrieve surface, atmospheric thermodynamic, and cloud microphysical parameters. A fast radiative transfer model, which applies to the clouded atmosphere, is used for atmospheric profile and cloud parameter retrieval. A one-dimensional (1-d) variational multi-variable inversion solution is used to improve an iterative background state defined by an eigenvector-regression-retrieval. The solution is iterated in order to account for non-linearity in the 1-d variational solution. It is shown that relatively accurate temperature and moisture retrievals can be achieved below optically thin clouds. For optically thick clouds, accurate temperature and moisture profiles down to cloud top level are obtained. For both optically thin and thick cloud situations, the cloud top height can be retrieved with relatively high accuracy (i.e., error < 1 km). NPOESS Airborne Sounder Testbed – Interferometer (NAST-I) retrievals from the Atlantic-THORPEX Regional Campaign are compared with coincident observations obtained from dropsondes and the nadir-pointing Cloud Physics Lidar (CPL). This work was motivated by the need to obtain solutions for atmospheric soundings from infrared radiances observed for every individual field of view, regardless of cloud cover, from future ultraspectral geostationary satellite sounding instruments, such as the Geosynchronous Imaging Fourier Transform Spectrometer (GIFTS) and the Hyperspectral Environmental Suite (HES). However, this retrieval approach can also be applied to the ultraspectral sounding instruments to fly on Polar satellites, such as the Infrared Atmospheric Sounding Interferometer (IASI) on the European MetOp satellite, the Cross-track Infrared Sounder (CrIS) on the NPOESS Preparatory Project and the following NPOESS series of satellites.

1. Introduction

Nadir observations from a spacecraft- or an aircraft-flown infrared instrument can be used to infer the atmospheric temperature, moisture, and concentration of other chemical species using radiative transfer equation inversion techniques. The retrievals of atmospheric state, temperature and moisture profiles, obtained from infrared radiometric measurements will contain intolerable error near and below the cloud level if the cloud radiation and the attenuation of infrared radiation emitted from the Earth's surface and the atmosphere below the clouds is not properly accounted for in the retrieval process. Clouds greatly complicate the interpretation of infrared sounding data. The new ultraspectral resolution infrared spectral radiance data contain the information needed to alleviate much of the ambiguity between cloud, atmospheric temperature, and moisture contributions which exists in lower spectral resolution sounding radiance data. Since there are vast cloudy regions of the globe, a great deal of effort has gone into cloud detection and cloud-clearing processes (Smith et al. 2004). Nevertheless, the schemes dealing with cloud detection and cloud-clearing (Smith 1968) remain a major source of error in the final retrieval products. Some schemes limit themselves to dealing with the observations unaffected by clouds (e.g., Chedin et al. 1985), while others make direct use of the cloudy radiances and attempt to retrieve temperature and moisture along with the cloud parameters (e.g., Susskind et al. 1984). Recently, fast molecular and cloud transmittance models (Huang et al. 2004) have been developed and used to retrieve cloud optical thickness from Atmospheric InfraRed Sounder (AIRS) measurements (Wei et al. 2004). The retrieval methodology is reliant on other cloud and thermodynamic parameters, such as cloud top pressure and atmospheric profiles of temperature, moisture, and ozone. Fast molecular and cloud transmittance models

have also been used to enable the infrared radiances to be used under cloudy conditions with the accuracy required for sounding retrieval processing; the EOF (empirical orthogonal function) statistical regression retrieval algorithm (e.g., Smith and Woolf 1976; Zhou et al. 2002) has been expanded to include realistic cloud parameters (e.g., cloud top height, effective particle diameter, and optical thickness) to deal with cloudy as well as cloud-free observations (Smith et al. 2004; Zhou et al. 2005a). With that recently developed EOF regression algorithm, cloud parameters as well as atmospheric profiles are retrieved simultaneously from infrared (IR) spectral radiance observations.

The NPOESS (National Polar-orbiting Operational Environmental Satellite System) Airborne Sounder Testbed – Interferometer (NAST-I) has been successfully operating on high altitude aircraft since 1998 (e.g., Cousins and Smith 1997; Smith et al. 2005). NAST-I is designed to support the development of future satellite temperature and moisture sounders such as the Infrared Atmospheric Sounding Interferometer (IASI) on the MetOp satellite, the Cross-track Infrared Sounder (CrIS) on the NPOESS Preparatory Project (NPP) and the following NPOESS series of satellites, as well as the GIFTS and the HES designed to fly on geostationary satellites. For obtaining dynamics (i.e., moisture flux and winds) from geostationary ultraspectral infrared radiance data, atmospheric profiles must be retrieved for every field of view, regardless of cloud cover, in order to obtain motion measurements from a time sequence of the 3-dimensional images of the atmospheric state variables (i.e., contiguous and continuous retrieval data are needed to construct the 3-dimensional images). Here we report that a physical retrieval scheme is developed to further improve retrieval accuracy based on EOF regressions. The physical retrieval scheme is described alone with the retrieval results for demonstration. Retrieval results of cloud and atmospheric properties from NAST-I observations are compared

with coincident observations obtained from the nadir-pointing Cloud Physics Lidar (CPL) and dropsondes, respectively.

2. Physical retrieval scheme

a. Radiative transfer model and Jacobian matrix

The radiance measurements within the short wavelength region, where the observed radiance may be affected by reflected solar radiation, are typically not used during daytime observing conditions. The cloud transmissive and reflective functions can be coupled with a fast molecular radiative transfer model. The NAST-I fast transmittance model used here is a combination of the Optimal Spectral Sampling (OSS) fast molecular radiative transfer model (Moncet et al. 2003; Liu et al. 2003) and the physically-based cloud radiative transfer model based on the DIScrete Ordinate Radiative Transfer (DISORT) (Stamnes et al. 1988) calculations performed for a wide variety of cloud microphysical properties (e.g., Yang et al. 2001; Huang et al. 2004). In the OSS approach, an extension of the Exponential Sum Fitting Transmittance method (Wiscombe and Evans 1977), radiance for each instrument channel is represented as a linear combination of radiances computed at a few pre-selected monochromatic frequencies within the domain spanned by the instrument line shape function (Moncet et al. 2003). Since the OSS model calculates channel radiances and transmittances at a few representative monochromatic frequencies, the top of atmosphere radiance for an atmosphere containing a single cloud layer is expressed by the monochromatic radiative transfer equation at those frequencies,

$$R = R_0 \, \mathrm{F_T} \, \tau_{tc} + R_c \tau_{tc} + R_\mathrm{l} + R_\mathrm{l}^{\downarrow} \, \mathrm{F_R} \, \tau_{tc} \,, \tag{1}$$

where R is the upwelling spectral radiance at the top of atmosphere. F_T and F_R are the cloud transmissive (including both direct and diffuse parts) and reflective (or albedo) functions, respectively. The terms R_0, R_c, R_1, and $R_1^{\downarrow}$ are upwelling emission below the cloud, emission from the cloud, upwelling emission above the cloud, and downwelling emission above the cloud, respectively. These terms are expressed below:

$$R_0 = \varepsilon \, \mathrm{B_s} \, \tau_{cs} + \int_{\tau_{cs}}^{1} \mathrm{B} \, d\tau + (1-\varepsilon) R_0^{\downarrow} \tau_{cs} \,, \tag{2}$$

$$R_0^{\downarrow} = \tau_{cs} \left(R_1^{\downarrow} \, \mathrm{F_T} + R_c \right) + \int_{\tau_{cs}}^{1} \mathrm{B} d\tau' \,, \tag{3}$$

$$R_c = \left(1 - \mathrm{F_R} - \mathrm{F_T}\right) \mathrm{B}(T_c) \,, \tag{4}$$

$$R_1 = \int_{\tau_{tc}}^{1} \mathrm{B} d\tau \,, \tag{5}$$

$$R_1^{\downarrow} = \int_{\tau_{tc}}^{1} \mathrm{B} d\tau' \,, \tag{6}$$

where ε refers to the Earth's surface emissivity, B is the Planck function, τ is the total transmittance from any given level to an upper boundary such as cloud level or the top of the atmosphere, and τ' is the total transmittance from any given level to a lower boundary such as cloud level or the Earth's surface. The transmittance between the cloud level and the Earth's surface is τ_{cs}, while τ_{tc} is the transmittance between the top of the atmosphere and cloud level. The subscripts s, c, and t denote the surface, cloud, and top of atmosphere, respectively. Figure 1

illustrates the various terms described above. It is noted that the top of atmosphere is assumed to be at the aircraft altitude for applications with the NAST airborne data. The transmissive and reflective functions at a given wavelength are taken from the pre-calculated database. In this study, particle habits are assumed to be hexagonal columns. Examples of cloudy radiance spectra simulated by the NAST-I forward radiative transfer model against cloud-free conditions are illustrated in Figure 2, showing different cloud features are captured mostly in the long wavelength window regions.

The cloud phase (i.e., clear, liquid, and ice cloud) is simply defined according to the retrieval. In other words, retrieved cloud top temperature determines whether the cloud is liquid or ice. The relationship between the optical thickness, ice water path, and particle size is simplified by the relationship between the ice water path and cloud optical thickness based on the parameterization of the balloon and aircraft cloud microphysical database (Heymsfield et al. 2003). Here, a simplified relation is used to specify cloud effective particle diameter from the cloud optical thickness,

$$D_e = \frac{a\xi_{vis}^{w}}{(\xi_{vis} - b\xi_{vis}^{w})}, \tag{7}$$

where a, b, and w are constants; D_e is the effective cloud particle diameter; and ξ_{vis} (later just ξ) is the visible optical thickness of the cloud. Two key cloud parameters, namely cloud top pressure and cloud optical thickness, remain in the regression and the first part of the physical iteration inversion. The weighting functions (or Jacobian matrixes) for cloud parameters are computed by a numerical perturbation method while others are computed by an analytical scheme. NAST-I analytical Jacobian matrixes for temperature, water vapor, and skin

temperature were computed as shown in Zhou et al. (2002). The numerical Jacobian matrix for cloud top pressure and optical thickness are expressed as

$$A_{ij} = \frac{[R_i(\psi_j) - R_i(\psi_j - \delta\psi_j)]}{\delta\psi_j}, \tag{8}$$

where i is channel index, j is cloud parameter ψ index (ψ_1 is cloud top pressure and ψ_2 is cloud optical thickness), and R is the simulated spectral radiance. An example of cloud parameter Jacobian is shown in Figure 3. The different spectral distributions of these weighting functions indicate the different channel radiance sensitivity and/or response to the cloud height and optical thickness.

b. Inversion scheme

An iterative eigenvector-regression-retrieval scheme was initially developed and used for retrieval analyses on both thermodynamic profiles and cloud parameters. These regression retrievals were compared with CPL and dropsonde data indicating a favorable agreement. Once the first guess is generated from the regression technique described by Zhou et al. (2005a), a non-linear iterative procedure is set up to produce a retrieval that is an improvement of the first guess (i.e., the EOF regression retrieval results). A one dimensional (1-d) variational solution, also known as the regularization algorithm or the minimum information method (e.g., Twomey 1963; Tikhonov 1963; Rodgers 1976; Hansen 1998), is chosen for NAST-I physical retrieval methodology which uses the regression solution as the initial guess. This solution has been applied to NAST-I radiances for retrieving both thermodynamic parameters and trace gases under cloud-free conditions (Zhou et al. 2002; Zhou et al. 2005b). Here, we expand the same

methodology to include cloud parameters dealing with retrieval problems under both cloudy and cloud-free conditions.

If the NAST-I observed radiance R_v^m of each channel is known, then R_v^m can be considered as a non-linear function of the atmospheric temperature profile (T), water vapor mixing ratio profile (q), surface skin temperature (T_s), surface emissivity (ε), cloud top pressure (P_c), effective cloud particle diameter (D_e), cloud visible optical-thickness (ξ), cloud phase (ϕ), etc. Therefore R_v^m equals $R_v(T, q, T_s, \text{å}, P_c, D_e, \xi, \phi, ...) + \sigma_v$, where σ_v is the instrument plus other sources of noise. Notice that D_e is initially a function of ξ as in Eq. (7). In general,

$$\mathbf{Y}^m = \mathbf{Y}(\mathbf{X}) + \sigma, \tag{9}$$

where the state vector **X** contains atmospheric temperatures, atmospheric moisture mixing ratios, surface skin temperature, cloud optical thickness, cloud top height, etc. $\mathbf{Y}^m$ contains N (number of channels used) observed radiances. The linear form of Eq. (9) is

$$\text{ä}\mathbf{Y} = \mathbf{Y}' \text{ä}\mathbf{X}, \tag{10}$$

where $\mathbf{Y}'$ (or $\mathbf{A}$) is the linear tangent of the forward model $\mathbf{Y}$ (or $\mathbf{R}$), the weighting function (or Jacobian) matrix. Here the linear model $\mathbf{Y}'$ uses an efficient analytical form (Li et al. 2000) for thermodynamic parameters and a numerical perturbation method for cloud parameters. A general form of the 1-d minimum variance solution minimizes the following penalty function (Rodgers 1976),

$$\mathbf{J}(\mathbf{X}) = [\mathbf{Y}^m - \mathbf{Y}(\mathbf{X})]^{\mathrm{T}} \mathbf{E}^{-1} [\mathbf{Y}^m - \mathbf{Y}(\mathbf{X})] + [\mathbf{X} - \mathbf{X}_0]^{\mathrm{T}} \mathbf{H} [\mathbf{X} - \mathbf{X}_0], \tag{11}$$

where superscript T denotes the transpose. Using the Newtonian iteration,

$$\mathbf{X}_{\mathrm{n+1}} = \mathbf{X}_{\mathrm{n}} + \mathbf{J}''(\mathbf{X}_{\mathrm{n}})^{-1} \mathbf{J}'(\mathbf{X}_{\mathrm{n}}), \tag{12}$$

the following Quasi-Nonlinear iterative form (Eyre 1989) is obtained:

$$\text{ä}\mathbf{X}_{\mathrm{n+1}} = (\mathbf{Y}_{\mathrm{n}}'^{\mathrm{T}} \mathbf{E}^{-1} \mathbf{Y}_{\mathrm{n}}' + \mathbf{H})^{-1}\, \mathbf{Y}_{\mathrm{n}}'^{\mathrm{T}}\, \mathbf{E}^{-1}\, (\text{ä}\mathbf{Y}_{\mathrm{n}} + \mathbf{Y}_{\mathrm{n}}' \text{ä}\mathbf{X}_{\mathrm{n}}), \tag{13}$$

where $\text{ä}\mathbf{X}_{\mathrm{n}} = \mathbf{X}_{\mathrm{n}} - \mathbf{X}_0$, $\text{ä}\mathbf{Y}_{\mathrm{n}} = \mathbf{Y}^{\mathrm{m}} - \mathbf{Y}(\mathbf{X}_{\mathrm{n}})$, $\mathbf{X}$ is the thermodynamic and cloud parameters to be retrieved, $\mathbf{X}_0$ is the initial state of these parameters or the first guess, $\mathbf{Y}^m$ is the vector of the observed radiances or brightness temperatures used in the retrieval process, **E** is the observation error covariance matrix which includes instrument noise and forward model error, and **H** is the *a priori* matrix which constrains the solution. Here, **H** can be the inverse of the *a priori* first guess error covariance matrix or another type of matrix. If the statistics of both the measurement and *a priori* error covariance matrix are Gaussian, then the maximum likelihood solution is obtained. However, if the *a priori* error covariance matrix is not known or is estimated incorrectly, the solution will be suboptimal (Eyre 1989). Here we apply $\mathbf{H} = \tilde{a}\mathbf{I}$ in Eq. (13), where γ is a Lagrangian multiplier which serves as a smoothing factor. Eq. (13) becomes

$$\text{ä}\mathbf{X}_{\mathrm{n+1}} = (\mathbf{Y}_{\mathrm{n}}'^{\mathrm{T}} \mathbf{E}^{-1} \mathbf{Y}_{\mathrm{n}}' + \tilde{a}\mathbf{I})^{-1}\, \mathbf{Y}_{\mathrm{n}}'^{\mathrm{T}}\, \mathbf{E}^{-1}\, (\text{ä}\mathbf{Y}_{\mathrm{n}} + \mathbf{Y}_{\mathrm{n}}'\, \text{ä}\mathbf{X}_{\mathrm{n}}), \tag{14}$$

which is commonly referred to as the minimum information solution. It is noted that γ is dependent upon the observations, the observation error, and the first guess of the atmospheric profile; often it is chosen empirically (e.g., Susskind et al. 1984; Smith et al. 1985; Hayden 1988). In the NAST-I retrieval procedure, the Discrepancy Principle (e.g., Morozov 1984; Carfora et al. 1998; Li and Huang 1999) is applied to determine the appropriate smoothing factor γ. Thus

$$\left\| \mathbf{Y}[\mathbf{X}(\gamma)] - \mathbf{Y}^{m} \right\|^{2} = \sigma^{2} \tag{15}$$

where $\sigma^2 = \sum_{\mathrm{k}=1}^{\mathrm{N}} e_k^2$, e_k is the square root of the diagonal of $\mathbf{E}$ or the observation error of channel k, which includes instrument error and forward model error. Error is shown in the equation, $e_{\mathrm{k}}^2 = \eta_{\mathrm{k}}^2 + f_{\mathrm{k}}^2$, where η_{k} is the instrument noise of channel k while f_{k} is the forward model error which is assumed to be 0.3 K for the same channel. Usually σ^2 can be estimated from the instrument noise and the validation of the atmospheric transmittance model used in the retrieval. Since Eq. (15) has a unique solution for γ (Li and Huang 1999), the atmospheric parameters and the smoothing factor can be determined simultaneously. In NAST-I retrieval processing, a simple numerical approach is adopted for solving Eq. (15); γ is changed in each iteration according to $\gamma_{\mathrm{n+1}} = q_{\mathrm{n}}\, \gamma_{\mathrm{n}}$, here q is a factor for γ increasing or decreasing. Based on Eq. (15), q is obtained in each iteration by satisfying the following conditions:

q_0=1.0;

if $\left\| \mathbf{Y}(\mathbf{X}_{\mathrm{n}}) - \mathbf{Y}^{\mathrm{m}} \right\| < \sigma^2$, then q_{n}=1.5;

if $\left\|\mathbf{Y}(\mathbf{X}_n) - \mathbf{Y}^m\right\| > \sigma^2$, then q_n=0.5;

if $\left\|\mathbf{Y}(\mathbf{X}_n) - \mathbf{Y}^m\right\| = \sigma^2$, then stop the iteration.

The q factor has been found from empirical experience to insure that the solution is stable between iterations. Thus, γ keeps changing until the iteration stops.

In the retrieval processing, several checks are made for retrieval quality control. The RMS (root-mean-square) of quantity $[\mathbf{Y}(\mathbf{X}_i) - \mathbf{Y}^m]$ from all selected channels χ_i is computed to check the convergence (or divergence). If $\chi_{i+1} > \chi_i$ within 2 iterations (i.e., iteration diverges), then the iteration is stopped and the retrieval is set to the first guess (or the previous atmospheric state); otherwise, iteration continues until χ_n <1.0K and $|\chi_n - \chi_{n-1}|$<0.01K, or a maximum of 10 iterations is reached. The degree of convergence of each iteration depends on the accuracy of the previous atmospheric and surface state. In addition, at each iteration, each level of the water vapor profile is checked for super-saturation. A unity magnitude of relative humidity is assumed at any super-saturated level.

The cloud particle size is derived using the relationship of Eq. (7) between the particle size and optical thickness. This relationship plays an influential role in both regression retrieval and physical matrix inversion. However, this relationship may not be true from case to case; on the other hand, the cloud signatures are captured in the long wavelength window region as shown in Figure 2, illustrating that the radiance spectral slope is sensitive to particle size and radiance magnitude is sensitive to optical thickness. Therefore, cloud microphysical parameters, namely effective particle diameter and visible optical thickness, are further refined with the radiances observed within the 10.4 μm to 12.5 μm window region, similar to what was described by Wei et al. (2004). The fitting of the magnitude and spectral slope of the radiance spectrum within the

window region is important for refining the cloud microphysical parameters. If these cloud parameters vary by more than 10% during this stage, the matrix inversion is performed again to produce atmospheric temperature and moisture profiles. To summarize this hybrid inversion scheme, a simplified flowchart is shown in Figure 4.

3. Case study and validation

NAST-I instrumentation, measurements, calibration, and radiance validation are documented elsewhere (e.g., Cousins and Smith 1997; Smith et al. 1999; Larar et al. 2002; Smith et al. 2005). NAST-I provides relatively high spectral resolution (0.25 cm^{-1}) measurements in the spectral region of 645–2700 cm^{-1} with moderate spatial resolution (a linear resolution equal to 13% of the aircraft altitude at nadir) cross track scanning. While a large amount of data has been collected since 1998 under a variety of meteorological conditions, results from only a very limited data set are presented herein for the purpose of "cloudy" retrieval demonstration. Retrievals from the Atlantic-THORPEX Regional Campaign (ATReC) (e.g., Shapiro and Thorpe 2004) are used to demonstrate this inversion methodology. These data, together with the radiosondes and dropsondes released from the NOAA G-4 aircraft that flew below the NASA ER-2 aircraft, provide a unique data set for detailed analysis of retrieval resolution and accuracy. During this field campaign, cloud properties were also provided by the nadir-pointing Cloud Physics LIDAR (CPL) on board the NASA ER-2 aircraft (McGill et al. 2002). All coincident observations obtained during this experiment are used to understand the atmospheric state and cloud microphysical properties for validating NAST-I retrievals.

The experiment of 5 December 2003 is chosen to test and demonstrate this inversion scheme with a realistic cloud radiative transfer model. The target scenes (latitude from 32ºN to

42ºN, longitude from 68ºW to 76ºW), shown in Figure 5, covered a variety of conditions desired by the scientific objectives of the experiment. These included a variety of cloud conditions, such as medium-level altocumulus, as well as low-level cumulus, thunderstorm, and extensive high cirrus in the ATReC region covered by the ER-2 and G-4 aircraft. The EOF regression retrievals have already shown reasonable agreement with the dropsondes and CPL observations (Zhou et al. 2005a). Here, the improvements through the physical retrieval scheme described above are emphasized by the demonstration of both radiance fitting and retrieval parameter validation.

a. Physical retrieval results and validation

The physical retrieval results of cloud and thermodynamic parameters are shown in Figure 6. NAST-I retrieved cloud top height (H_c) from the nadir observations against CPL measured cloud top heights of the top 2 layers; and Figure 6b shows the cloud optical thickness inferred from NAST-I measurements against that of the CPL 1064 nm channel measurements. It is noted that NAST-I spatial resolution (at the cloud height and at nadir) is 13% of the distance between the aircraft altitude and the cloud height (i.e., 1.56 km when the cloud height is at 8 km and the ER-2 is at 20 km), while the CPL horizontal resolution is about 0.2 km; furthermore, the NAST-I vertical resolution is about 1 km while the CPL vertical resolution is 0.03 km. Despite the differences of the instruments and of their spatial resolutions, the cloud top heights inferred from NAST-I compare very well with CPL measurements for the variety of cloud conditions observed. The measurement sensitivity and accuracy of cloud optical thickness inferred from the infrared measurement is expected to be much poorer than that measured by the CPL because of the spatial resolution differences between the two instruments. Even so, NAST-I cloud optical thickness retrievals compare favorably to CPL observations.

NAST-I retrieved temperature and relative humidity (RH) vertical cross sections are shown in Figure 6d and 6e, respectively. The areas whited out are under the clouds where the cloud optical thickness is larger than one. The variation of atmospheric conditions is captured very well by NAST-I retrievals, not only for the clear regions above optically thick clouds, but also for regions below optically thin clouds. These soundings are also validated by the dropsondes released from the G-4 aircraft. The dropsondes are used to reveal the retrieval sounding accuracy under cloudy conditions. Inter-comparisons between each dropsonde and NAST-I local mean (i.e., 5×5 single field of views) retrieval are presented in Figure 7. In general, the retrievals show a good agreement above the clouds; the sounding comparison continues to show a good agreement under the optically thin clouds to the second layer clouds as is indicated by the CPL observations, and retrievals are relatively accurate under the optically thin clouds. The erroneous retrievals below opaque clouds are shown. These errors, which were due to the limitation of infrared observations, were expected and should be discarded. As shown in Figures 6 and 7, retrievals of temperature and moisture above the clouds are not disturbed by the clouds below. Both temperature and relative humidity profiles show a continuity variation from time to time (i.e., from location to location) indicating that the atmospheric features are well captured by NAST-I observations and retrievals.

b. Improved with physical inversion

The regression retrievals with realistic cloudy radiance training have already shown the improvement over the clear and/or isothermal equivalent radiance training (Zhou et al. 2005a). However, the physical inversion scheme further improves the retrieval accuracy from the cloudy iteration-regression. Figure 8 shows the deviation of retrieved parameters from the regression to

the physical algorithms used. Several approaches are used herein to show the retrievals are evidently improved through physical inversion. The cloud particle size is produced as a function of optical thickness in order to reduce a number of retrieval parameters in the regression process, which results in an artificial correlation between these parameters as in Eq. (7). Plotted in Figure 9 are the retrieval results from regression (gray dots) to physical (black dots), the physical outcomes still obey the prediction of Eq. (7) but with expected scattering.

The cloud parameters retrieved from NAST-I observations plotted in Figure 6 indicate that a variety of cloud conditions were also observed by the GOES-8 visible and infrared imaging sensors (Figure 5). The radiance fitting statistics over this large diversity data set gives a clear reflection on the integrity of this retrieval algorithm. A few thousand NAST-I observations (all nadir of 5 December 2003 flight) are used to compare with their associated retrieval simulations in order to show retrieval accuracy. The standard deviation error (STDE) and mean bias in brightness temperature are plotted in Figure 10; the retrieval accuracy is improved significantly through the physical inversion. The relatively large error in the short wavelength region (i.e., wavenumber greater than 2200 cm^{-1}) is mainly due to NAST-I instrument noise, solar component not accounted for in the simulation, and the cloud model was cut off at a wavenumber of 2500 cm^{-1}. Despite the uncertainty of the radiative transfer model (especially in the short wavelength region), the STDE from the physical retrieval is more like the instrument noise estimated from instrument calibration. This improvement evidently indicates that retrieved parameters, in general, are accurately retrieved through this physical inversion scheme.

Finally, spectral radiance comparisons of individual scans have also been examined over each dropsonde location where the temperature and moisture profiles can be validated to ensure

that the deviations shown in Figure 8 are in favor of approaching the real atmospheric conditions through the physical inversion. Two samples, the first and 7th dropsondes indicated in Figure 6d, are shown in Figures 11 and 12, respectively. Again, the radiance and retrieved parameters were compared to show the integrity of the algorithm. Panels (a) and (b) illustrate the radiance convergence to NAST-I observation, while (c), (d), and (e) show the temperature and moisture convergence to the dropsonde through the physical inversion. The retrieved cloud parameters are indicated in the figure captions.

4. Concluding remarks

Our previous regression results indicate some success in the ability to retrieve information below scattered and partially transparent cirrus clouds, or clouds with an effective optical thickness of less than one. The initial EOF regression has laid a first step in dealing with infrared sounding data under cloudy conditions, which is now significantly improved by the physical iteration inversion described in this study. Results achieved with airborne NAST-I observations show that accuracies close to those achieved in totally cloud-free conditions can be achieved down to cloud top levels. The accuracy of the profile retrieved below cloud top level is dependent upon the optical thickness and fractional coverage of the clouds. Retrieval accuracy of temperature and moisture profiles is greatly improved by the physical inversion as shown by dropsonde validation. Therefore, the radiances can be accurately simulated by using physically inverted results, which is important for direct assimilation into a forecast model. The thermodynamic profile information might be obtained through a combination of cloud clearing and direct retrieval from the clouded radiances using a realistic cloud radiative transfer model. The correct implementation still requires a considerable research development effort; however,

cloudy sky radiative transfer models should enable the extraction of profile information from cloud contaminated radiances suitable for numerical weather prediction application.

Acknowledgments. The NAST-I program is supported by the NPOESS Integrated Program Office (IPO), NASA Headquarters, and NASA Langley Research Center. The authors also acknowledge support from NASA Headquarters Research Division Director Dr. Jack Kaye and IPO Program Manager Dr. Karen St.Germain. The authors express sincere thanks to the NAST-I team members from various organizations. The CPL data were kindly provided by Dr. Matthew J. McGill of NASA Goddard Space Flight Center. The fast cloud radiative transfer model was provided by Dr. Ping Yang of Texas A&M University. The OSS molecular radiative transfer model was provided by the Atmospheric and Environmental Research, Inc.

REFERENCES

Carfora, M. F., F. Esposito, and C. Serio, 1998: Numerical methods for retrieving aerosol size distributions from optical measurements of solar radiation, *J. Aerosol Sci.*, **29**, 1225–1236.

Chedin, A., N. A. Scoot, C. Wahiche, and P. Moulinier, 1985: The improved initialization inversion method: a high resolution physical method for temperature retrievals from the TIROS-N series, *J. Appl. Meteor.*, **24**, 128–143.

Cousins, D., and W. L. Smith, 1997: National Polar-Orbiting Operational Environmental Satellite System (NPOESS) Airborne Sounder Testbed-Interferometer (NAST-I), *Proc. SPIE* **3127**, 323–331.

Eyre, J. R., 1989: Inversion of cloudy satellite sounding radiances by nonlinear optimal estimation. I: Theory and simulation for TOVS, *Quart. J. Roy. Meteor. Soc.*, **115**, 1001–1026.

Hansen, P. C., 1998: *Rank-Deficient and Discrete Ill-Posed Problems: Numerical Aspects of Linear Inversion*. SIAM, 247 pp.

Hayden, C. M., 1988: GOES-VAS simultaneous temperature-moisture retrieval algorithm, *J. Appl. Meteor.*, **27**, 705–733.

Heymsfield, A. J., S. Matrosov, and B. Baum, 2003: Ice water path–optical depth relationships for cirrus and deep stratiform ice cloud layers, *J. Appl. Meteor.*, **42**, 1369–1390.

Huang, H.-L., P. Yang, H. Wei, B.A. Baum, Y. X. Hu, P. Atonelli, and S. A. Ackerman, 2004: Inference of ice cloud properties from high-spectral resolution infrared observations. *IEEE Trans. Geosci. Remote Sensing*, **42**, 842–852.

Larar, A. M., W. L. Smith, and D. K. Zhou, 2002: Spectral radiance validation studies using NAST-I and other independent measurement systems, *Proc. SPIE*, **4485**, 81–90.

Li, J., and H. L. Huang, 1999: Retrieval of atmospheric profiles from satellite sounder measurements using the discrepancy principle, *Appl. Opt.*, **38**, 916–923.

Li, J., W. W. Wolf, W. P. Menzel, W. Zhang, H. L. Huang, and T. H. Achtor, 2000: Global soundings of the atmosphere from ATOVS measurements: The algorithm and validation, *J. Appl. Meteor.*, **39**, 1248–1268.

Liu, X., J.-L. Moncet, D. K. Zhou, and W. L. Smith, 2003: A Fast and Accurate Forward Model for NAST-I Instrument, in *Fourier Transform Spectroscopy and Optical Remote Sensing of Atmosphere,* 2003 Technical Digest Series OSA (Optical Society of America, Washington, D.C., 2003), p. 16.

McGill, M. J., D. L. Hlavka, W. D. Hart, J. D. Spinhirne, V. S. Scott, and B. Schmid, 2002: The Cloud Physics Lidar: Instrument description and initial measurement results, *Appl. Opt.,* **41**, 3725–3734.

Moncet, J. L., and Coauthors, 2003: Algorithm theoretical basis document (ATBD) for the Cross Track Infrared Sounder (CrIS) environmental data records (EDR), V1.2.3, *AER Document Number P882-TR-E-1.2.3-ATBD-03-01*.

Morozov, V. A., 1984: *Methods for solving incorrectly posed problems*. Springer-Verlag, 257 pp.

Rodgers, C. D., 1976: Retrieval of atmospheric temperature and composition from remote measurements of thermal radiation, *Rev. Geophys. Space Phys.,* **14**, 609–624.

Shapiro, M. A., and A. J. Thorpe, 2004: THORPEX: A global atmospheric research program for the beginning of the 21st century, *WMO Bulletin*, **53**, 222–226.

Smith, W. L., 1968: An improved method for calculating tropospheric temperature and moisture from satellite radiometer measurements, *Mon. Wea. Rev.*, **96**, 387–396.

Smith, W. L., and H. M. Woolf, 1976: The use of eigenvectors of statistical co-variance matrices for interpreting satellite sounding radiometer observations, *J. Atmos. Sci.,* **33**, 1127–1140.

Smith, W. L., H. M. Woolf, C. M. Hayden, and A. J. Schreiner, 1985: The simultaneous export retrieval package, *Tech. Proc. Second Int. TOVS Study Conf.*, Igls, Austria, CIMSS, 224–253.

Smith, W. L., A. M. Larar, D. K. Zhou, C. A. Sisko, J. Li, B. Huang, H. B. Howell, H. E. Revercomb, D. Cousins, M. J. Gazarik, D. Mooney, 1999: NAST-I: results from revolutionary aircraft sounding spectrometer, *Proc. SPIE,* **3756**, 2–8.

Smith, W. L., D. K. Zhou, A. M. Larar, S. A. Mango, H. B. Howell, R. O. Knuteson, H. E, Revercomb, and W. L. Smith Jr., 2005: The NPOESS Airborne Sounding Testbed Interferometer – remotely sensed surface and atmospheric conditions during CLAMS, *J. Atmos. Sci.*, **62**, 1117–1133.

Smith, W. L., D. K. Zhou, H.-L. Huang, J. Li, X. Liu, and A. M. Larar, 2004: Extraction of profile information from cloud contaminated radiances, paper presented at the ECMWF Workshop on the Assimilation of High Spectral Resolution Sounders in NWP, June 28 – July 1, 2004.

Stamnes, K., S.-C. Tsay, W. Wiscombe, and K. Jayaweera, 1988: Numerically stable algorithm for discrete-ordinate-method radiative transfer in multiple scattering and emitting media, *App. Opt.*, **27**, 2502–2509.

Susskind, J., J. Rosenfield, D. Reuter, and M. T. Chadine, 1984: Remote sensing of weather and climate parameters from HIRS2/MSU on TIROS-N, *J. Geophys. Res*., **89**, 4677–4697.

Tikhonov, A. N., 1963: On the solution of incorrectly stated problems and a method of regularization, *Dokl. Acad. Nauk. SSSR,* **151**, 501–504.

Twomey, S., 1963: On the numerical solution of Fredholm integral equations of the first kind by inversion of the linear system produced by quadrature, *J. Ass. Comput. Mach.,* **10**, 97–101.

Wei, H., P. Yang, J. Li, B. A. Baum, H.-L. Huang, S. Platnick, Y. Hu, and L. Strow, 2004: Retrieval of ice cloud optical thickness from Atmospheric Infrared Sounder (AIRS) measurements. *IEEE Trans. Geosci. Remote Sensing*, **42**, 2254–2265.

Wiscombe W. J., and J. W. Evans, 1977: Exponential-sum fitting of radiative transmission functions, *J. Comput. Phys.,* **24**, 416–444.

Yang, P., B. C. Gao, B. A. Baum, Y. Hu, W. J. Wiscombe, S.-C. Tsay, D. M. Winker, S. L. Nasiri, 2001: Radiative Properties of cirrus clouds in the infrared (8-13 μm) spectral region, *J. Quant. Spectros. Radiat. Transfer*, **70**, 473–504.

Zhou, D. K., W. L. Smith, J. Li, H. B. Howell, G. W. Cantwell, A. M. Larar, R. O. Knuteson, D. C. Tobin, H. E. Revercomb, and S. A. Mango, 2002: Thermodynamic product retrieval methodology for NAST-I and validation, *App. Opt.*, **41**, 6957–6967.

Zhou, D. K., W. L. Smith, X. Liu, A. M. Larar, H.-L. A. Huang, J. Li, M. J. McGill, and S. A. Mango, 2005a: Thermodynamic and cloud parameters retrieval using infrared spectral data, *Geophys. Res. Lett*., **32**, L15805, doi:10.1029/2005GL023211.

Zhou, D. K., W. L. Smith, X. Liu, J. Li, A. M. Larar, and S. A. Mango, 2005b: Tropospheric CO observed with the NAST-I: retrieval methodology, analyses, and first results, *Appl. Opt.*, **44**, 3032–3044.

FIGURE CAPTIONS:

FIG. 1. Schematic illustrating the contributions to the simulated monochromatic radiance.

FIG. 2. Simulated NAST-I spectra with cloud-free (black) and different cloud conditions of ice cloud top pressure at 250 hPa: the blue curve indicates particle size (D_e) of 80 μm and optical thickness (ξ) of 0.5; the green curve indicates D_e of 80 μm and ξ of 0.1; the red curve indicates D_e of 10 μm and ξ of 0.1.

FIG. 3. The normalized absolute weighting functions of cloud top height (H_c at 6.8 km) and optical thickness.

FIG. 4. A simple flow diagram summarizing the physical retrieval scheme employed for cloudy and/or cloud-free spectral radiance.

FIG. 5. GOES-8 infrared image (at 18:30 UTC on 5 December 2003) showing a variety of cloudy conditions in the region covered by the NASA ER-2 and the NOAA G-4 aircraft. The ER-2 flight track is plotted over the GOES image. The dropsondes from the G-4 aircraft are also marked with asterisks (and a D#).

FIG. 6. Panel (a) plots NAST-I physically retrieved cloud top height compared with the CPL measured cloud top heights of the top 2 layers (L1 and L2). Panel (b) plots NAST-I retrieved visible cloud optical thickness (COT or ξ) compared with the CPL measurement. Panel (c) plots NAST-I retrieved cloud particle size. Panels (d) and (e) plot NAST-I physically retrieved temperature and relative humidity vertical cross sections, respectively. The areas wiped off are under the top layer clouds where the cloud visible optical thickness is larger than one and under the lower "opaque" cloud. The black vertical bars in panel (d) indicate dropsonde locations.

FIG. 7. Inter-comparisons between NAST-I local mean retrievals (red curve is above the cloud while green curve is below the cloud) and dropsondes (blue curve).

FIG. 8. The retrieved parameter deviates from the regression to physical retrievals, as demonstrated in the above plots of NAST-I physical minus regression retrievals.

FIG. 9. The correlation between cloud optical thickness and effected particle diameter: gray dots (formed a smooth curve) are from the regressions and black dots are produced from the physical retrievals.

FIG. 10. Spectral data consistency showing the retrieval accuracy (for all nadir observations of 5 December 2003 flight): (a) standard deviation error and (b) mean bias (simulated minus measured). The black and gray curves are produced from physical retrievals and regressions, respectively.

FIG. 11. Comparison of spectral radiance and retrievals of temperature and water vapor corresponding to cirrus ice clouds near the first dropsonde. The cloud parameters changed from regression are the H_c of 5.9 km from 6.8 km, ξ of 1.37 from 0.69, and D_e of 42.8 μm from 51.4 μm.

FIG. 12. Comparison of spectral radiances and retrievals of temperature and water vapor corresponding to cirrus ice clouds near the 7th dropsonde. The cloud parameters changed from regression are the H_c of 3.7 km from 5.4 km, ξ of 1.81 from 0.41, and D_e of 63.4 μm from 44.7 μm.

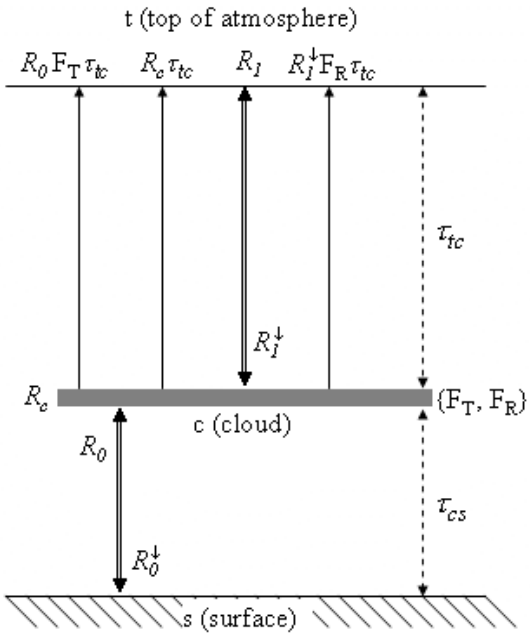

FIG. 1. Schematic illustrating the contributions to the simulated monochromatic radiance.

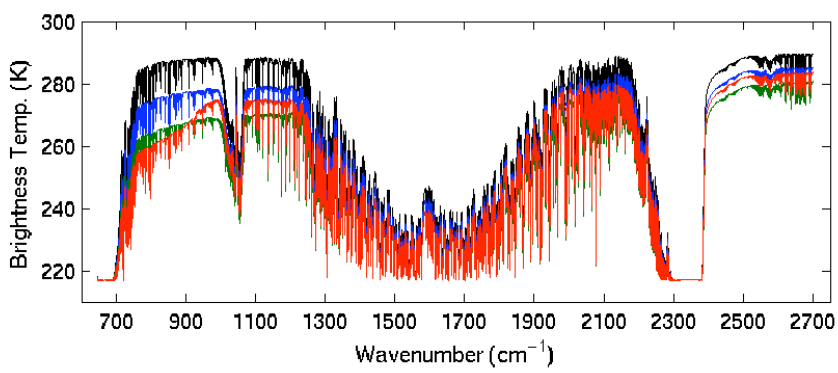

FIG. 2. Simulated NAST-I spectra with cloud-free (black) and different cloud conditions of ice cloud top pressure at 250 hPa: the blue curve indicates particle size (D_e) of 80 μm and optical thickness (ξ) of 0.5; the green curve indicates D_e of 80 μm and ξ of 0.1; the red curve indicates D_e of 10 μm and ξ of 0.1.

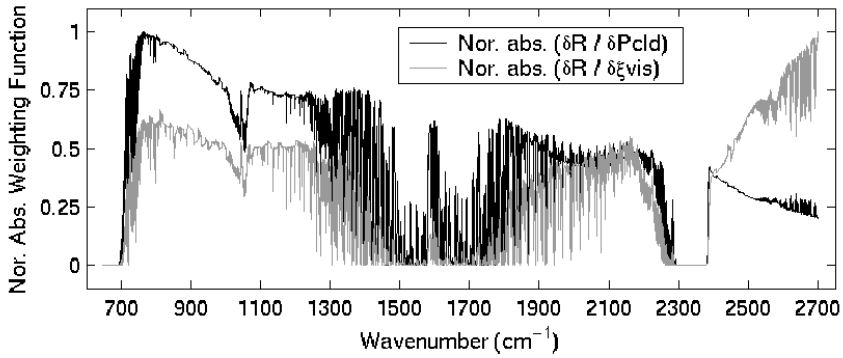

FIG. 3. The normalized absolute weighting functions of cloud top height (H_c at 6.8 km) and optical thickness.

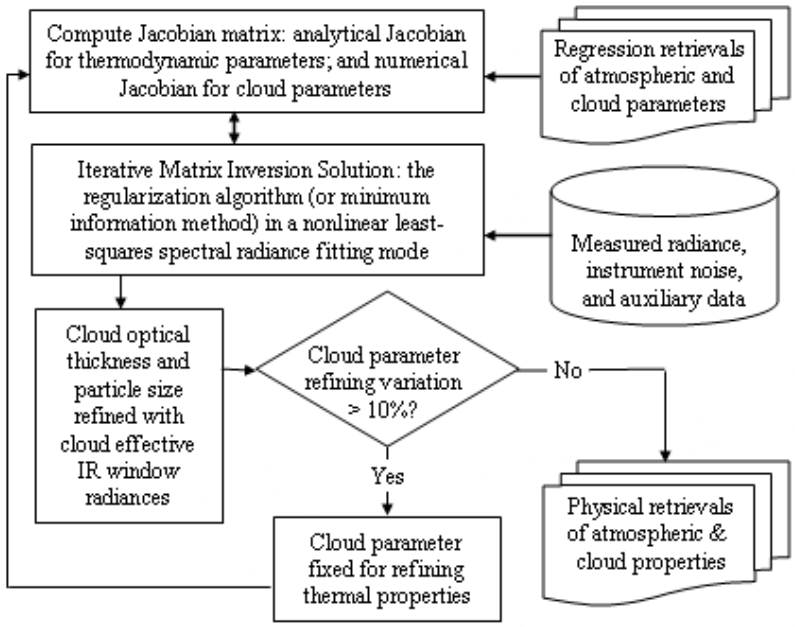

FIG. 4. A simple flow diagram summarizing the physical retrieval scheme employed for cloudy as well as cloud-free spectral radiance.

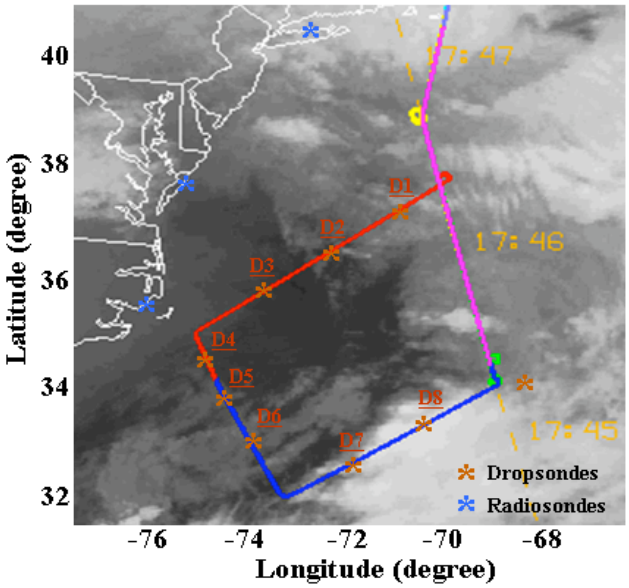

FIG. 5. GOES-8 infrared image (at 18:30 UTC on 5 December 2003) showing a variety of cloudy conditions in the region covered by the NASA ER-2 and the NOAA G-4 aircraft. The ER-2 flight track is plotted over the GOES image. The dropsondes from the G-4 aircraft are also marked with asterisks (and a D#).

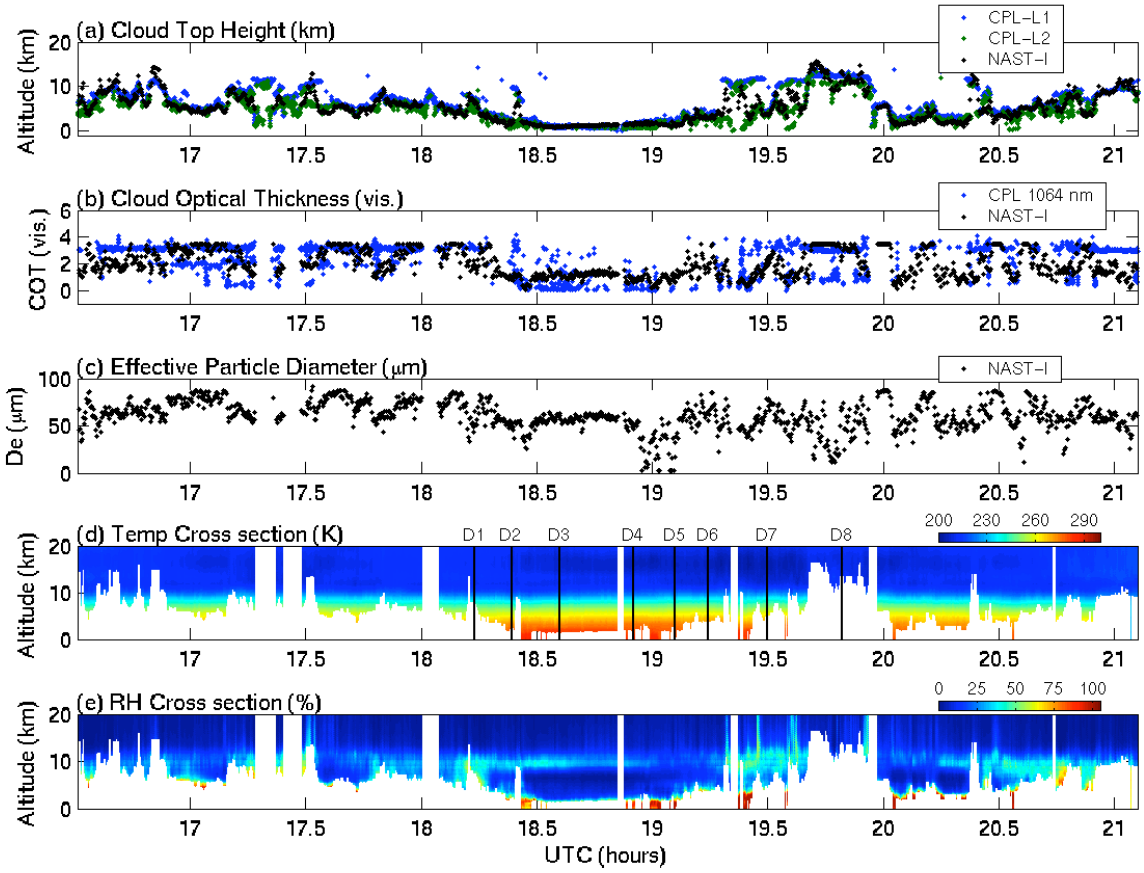

FIG. 6. Panel (a) plots NAST-I physically retrieved cloud top height compared with the CPL measured cloud top heights of the top 2 layers (L1 and L2). Panel (b) plots NAST-I retrieved visible cloud optical thickness (COT or ξ) compared with the CPL measurement. Panel (c) plots NAST-I retrieved cloud particle size. Panels (d) and (e) plot NAST-I physically retrieved temperature and relative humidity vertical cross sections, respectively. The areas wiped off are under the top layer clouds where the cloud visible optical thickness is larger than one and under the lower "opaque" cloud. The black vertical bars in panel (d) indicate dropsonde locations.

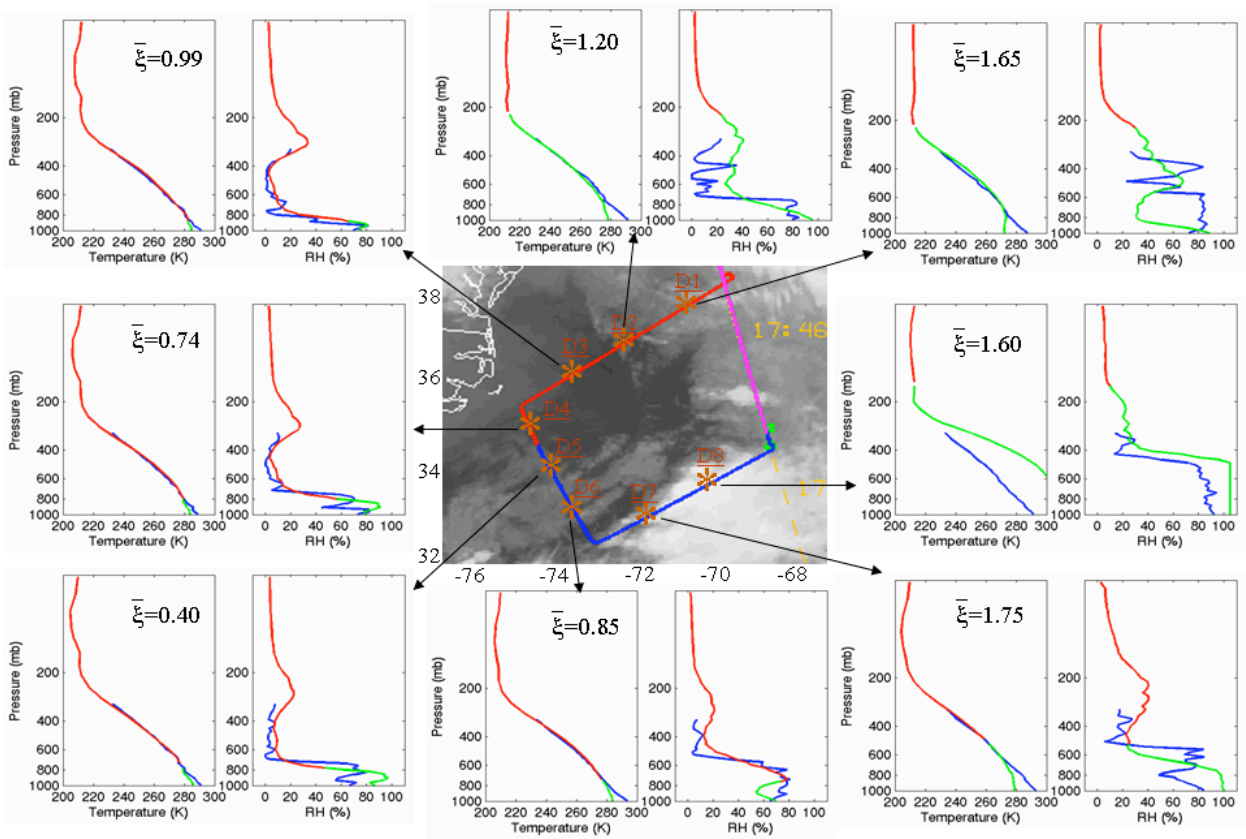

FIG. 7. Inter-comparisons between NAST-I local mean retrievals (red curve is above the cloud while green curve is below the cloud) and dropsondes (blue curve).

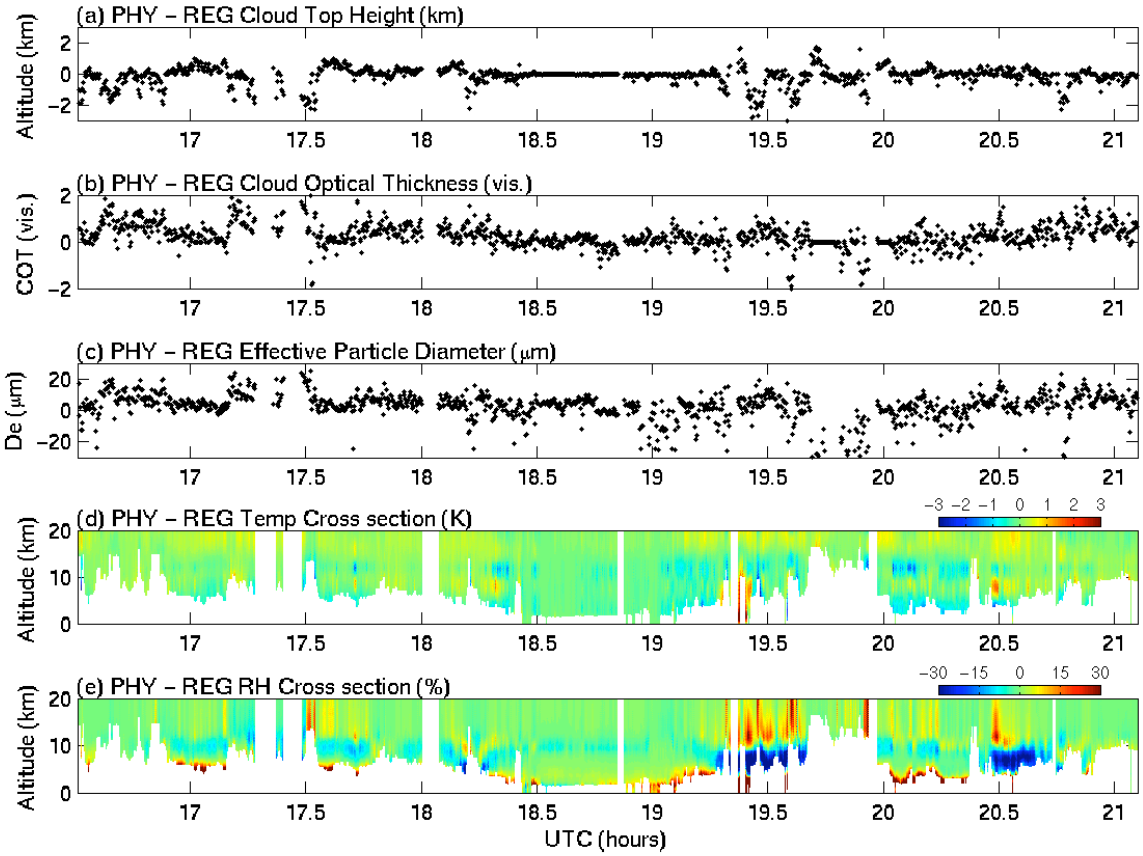

FIG. 8. The retrieved parameter deviates from the regression to physical retrievals, as demonstrated in the above plots of NAST-I physical minus regression retrievals.

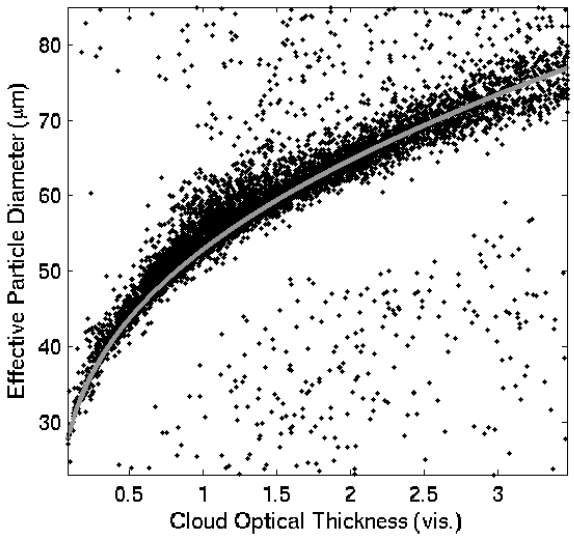

FIG. 9. The correlation between cloud optical thickness and effected particle diameter: gray dots (formed a smooth curve) are from the regressions and black dots are produced from the physical retrievals.

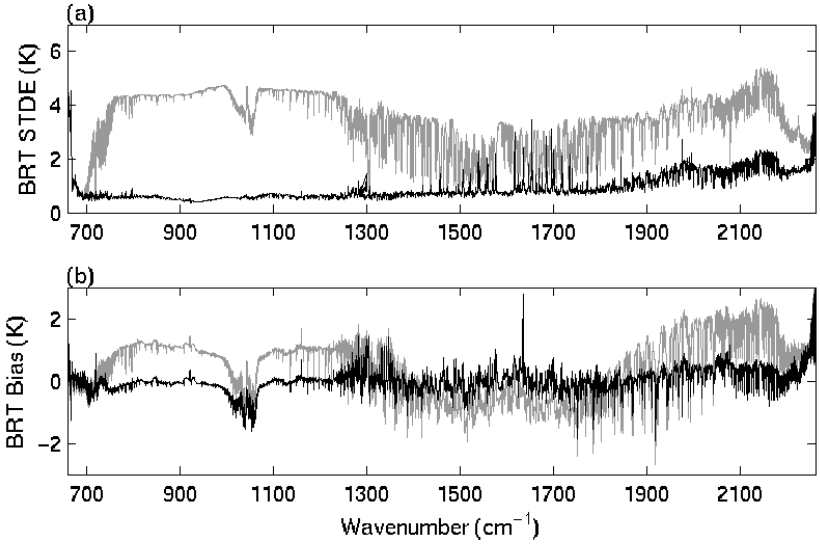

FIG. 10. Spectral data consistency showing the retrieval accuracy (for all nadir observations of 5 December 2003 flight): (a) standard deviation error and (b) mean bias (simulated minus measured). The black and gray curves are produced from physical retrievals and regressions, respectively.

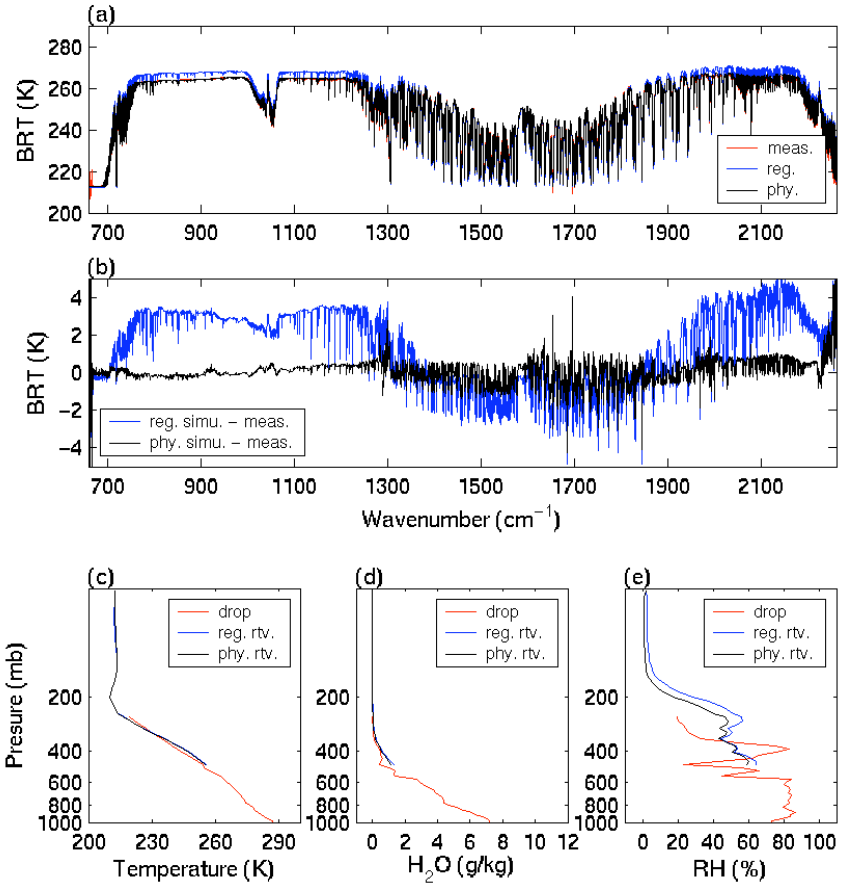

FIG. 11. Comparison of spectral radiance and retrievals of temperature and water vapor corresponding to cirrus ice clouds near the first dropsonde. The cloud parameters changed from regression are the H_c of 5.9 km from 6.8 km, ξ of 1.37 from 0.69, and D_e of 42.8 μm from 51.4 μm.

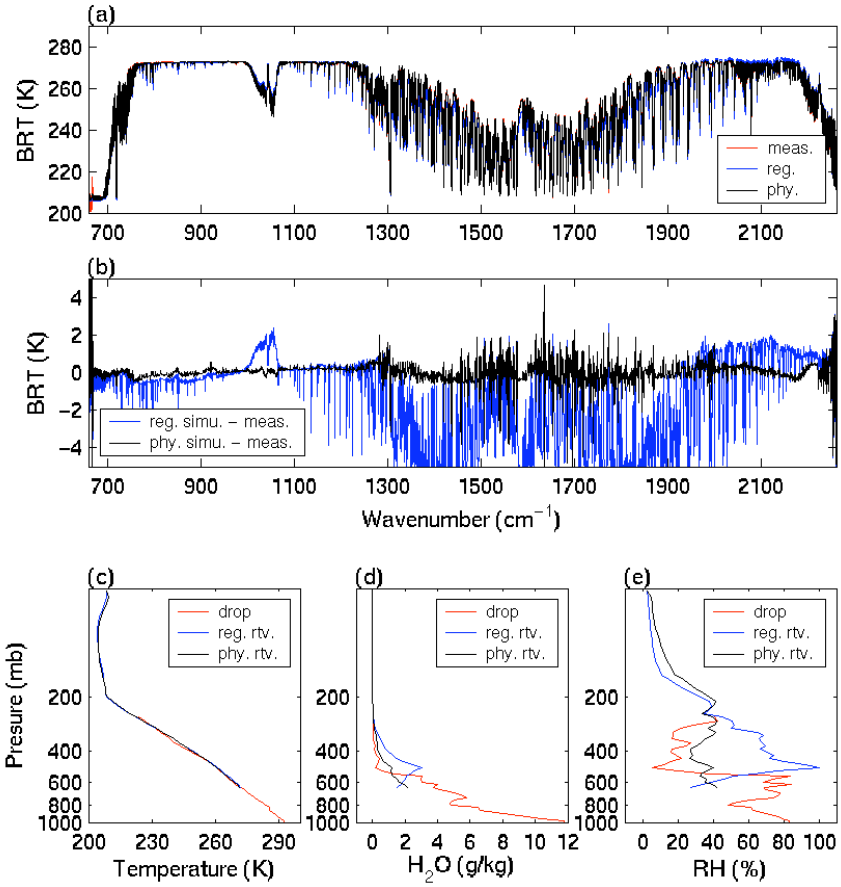

FIG. 12. Comparison of spectral radiances and retrievals of temperature and water vapor corresponding to cirrus ice clouds near the 7th dropsonde. The cloud parameters changed from regression are the H_c of 3.7 km from 5.4 km, ξ of 1.81 from 0.41, and D_e of 63.4 μm from 44.7 μm.